



PIV ANALYSIS OF MODE BIFURCATION IN TAYLOR VORTEX FLOW

H. FURUKAWA¹, H. HORIKOSHI¹, N. OHAZAMA¹, T. WATANABE²

¹Department of Mechanical Engineering, Meijo University, Nagoya, 468-8502, Japan

²Graduate School of Information Science, Nagoya University, Nagoya, 464-8601, Japan

^cCorresponding author: Tel.: +81528382327; Fax: +81528321235; Email: furukawa@meijo-u.ac.jp

KEYWORDS:

Main subjects: Taylor vortex flow

Fluid: water

Visualization method(s): PIV

Other keywords: bifurcation, time dependent flow

ABSTRACT: Since the classical investigation of the Taylor vortex by G. I. Taylor in 1923, many researchers have studied the Taylor vortex as one of the most important vortex types in flow. In this study, the inner cylinder is rotating, while the outer cylinder, which is concentric with the inner cylinder, is stationary. The phenomenon is visualized experimentally as a three-dimensional problem. In addition, the measurement of the velocity distribution is carried out by the PIV method. The radius of the inner cylinder is 20 mm, and that of the outer cylinder is 30 mm. The gap between the inner and outer cylinders is 10 mm. In this study, $Re = 650 - 1200$ is assumed. A pulley is attached to the belt wheel places at the bottom center of the apparatus in order to rotate the inner cylinder. In the upper part of the apparatus, movable ends are fixed to the upper and lower sides of the cylinder to change the aspect ratio. The aspect ratio Γ is defined as the ratio of cylinder height to gap distance. A servo motor to rotate the inner cylinder, a servo- motor control device, a servo amplifier for rotation speed control, and a YAG laser light source are installed in the apparatus. For the visualization of Taylor vortex flow, aluminum powder composed of scale like fine particles is used. The size of the aluminum particles is uniform at 20 micro meters. As tracer particles used in the PIV method, fluorescent particles with a size of 48 micro meters were used. The governing equations are Navier-Stokes equations with cylindrical coordinates (r , θ , z) and the equations of continuity. Each physical value is nondimensionalized using the angular velocity of the inner cylinder as the representative velocity, and the radius difference between the inner and outer cylinders as the representative length. Discretization of the governing equations is based on the MAC method. The results of EFD and CFD are compared. The mode bifurcation is observed, and the flow structure is investigated.

1. Introduction

Taylor vortex flow has been studied as an important vortex flow since it was first reported by G. I. Taylor in 1923. In a concentric double cylinder, when the rotation speed of the inner cylinder is gradually increased from zero, Couette flow first occurs in the gap between the inner and outer cylinders. When the rotation speed of the inner cylinder is further increased, Couette flow changes to Taylor vortex flow, in which many torus flows called cells are stacked, then to wavy Taylor vortex flow, and finally to turbulent flow. Taylor vortex flow often appears in journal bearings, hydrodynamic machines, and containers for chemical reactions, and clarification of the mechanism of Taylor vortex flow is highly important for the engineering field. Figure 1 shows a schematic of Taylor vortex flow.

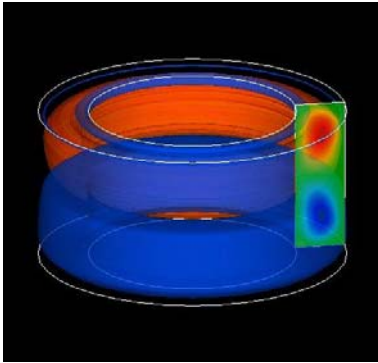


Fig.1 Taylor vortex flow

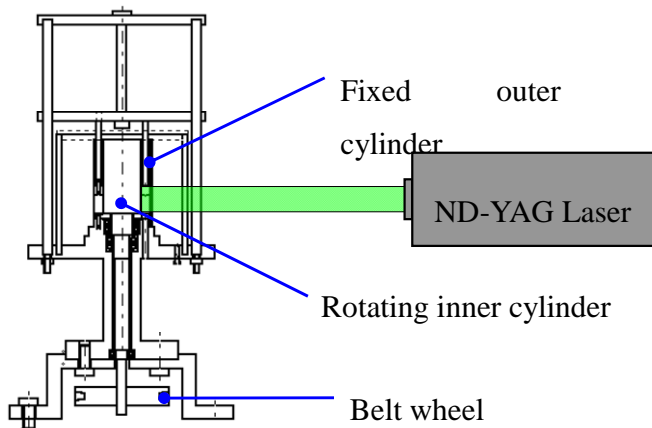


Fig.2 Schematic of experimental setup

The main parameters that govern Taylor vortex flow generated in concentric double cylinders of finite length are the aspect ratio, which is the ratio of the cylinder height to the width of the gap between the inner and outer cylinders, and the Reynolds number, which depends on the rotation speed of the inner cylinder. Various types of Taylor vortex flow are formed depending on these parameters. The structure of Taylor vortex flow is roughly classified into two modes: normal mode and anomalous mode. In the case of a concentric double cylinder with the upper and lower ends fixed, the normal mode exhibits inward flows from the outer cylinder to the inner cylinder at both the upper and lower ends.

In contrast, the anomalous mode exhibits outward flows at one or both ends of the cylinders. The purpose of this study is to analyze the transition processes of unsteady Taylor vortex flow by Particle Image Velocimetry (PIV). Moreover, the size of extra vortices generated during the transition process is measured and the anomalous one-cell mode is also analyzed by PIV.

2. Experimental Setup and Procedure

Figure 2 shows a schematic of the experimental setup used in this study. The radii of the inner and outer cylinders are $r_{in} = 20$ mm and $r_{out} = 30$ mm, respectively, and the gap between the cylinders is $r_{out} - r_{in} = 10$ mm. The inner cylinder is rotated at an angular velocity of ω . A pulley is attached to a belt wheel below the center of the cylinder to rotate the inner cylinder. Here, only the inner cylinder is rotated because the outer cylinder is fixed. A slide ring is attached to the upper ends of the cylinders to fix their positions and to change the aspect ratio of the gap, which is used as the observation target. The setup also includes a servo motor, a servo amplifier (MR-J2-A, Mitsubishi Electric Corporation), a servo motor control unit (Tateiwa Shoji), and a Nd-YAG laser device (1.5W, DSPP Green Laser, Japan Laser Corporation).

A mixture of distilled water and glycerin with a mixing ratio of 8:2 is used as the fluid specimen in this study. The specific gravity of glycerin is 1.26. The advantages of using glycerin are that (1) the Reynolds number can be controlled by varying its viscosity and (2) it helps tracer particles float in the fluid specimen. The tracer particles used in this study are fine fluorescent particles with a high luminescence, which were added to the fluid to visualize flows. FLUOSTAR (EBM Corporation) particles are used in this study. When laser light is irradiated onto these particles perpendicularly to the observation direction, flows can be observed owing to the reflection of light.

The aspect ratio was determined, and the rotation speed of the servo motor required to give the desired Reynolds number and the time required to reach this value (i.e., the rising time) were input to the servo amplifier. Next, the motor was driven and photographs were taken using a high-speed video camera



(VCC-H1000, Digimo Co., Ltd.) when the vortex stabilized to form the final-mode flow. The obtained video

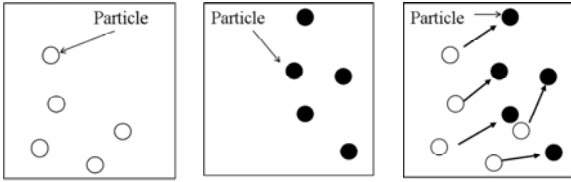


Fig.3 PIV Analytical method

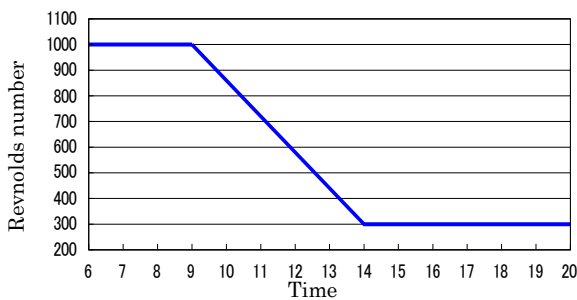


Fig.4 How to change in Re

data were sent to a PC and converted into a file of successive images, which were analyzed using two types of analytical software Koncerto (Seika Corporation). The parameters that govern Taylor vortex flow are the Reynolds number and aspect ratio, as mentioned above. The Reynolds number Re is a dimensionless number, defined as the ratio of the inertial force in the equation of motion to the viscous force, and is given by

$$Re = \frac{Vd}{\nu} \quad (1)$$

Here, V is a representative velocity, given as the rotation speed of the inner cylinder ($r_{in}\omega$), d is the width of the gap between the inner and outer cylinders, given by the difference between their representative radii as $r_{out} - r_{in}$, and ν is the kinematic viscosity of the fluid. The aspect ratio Γ is defined as the ratio of the cylinder length L to the gap width $r_{out} - r_{in}$, and is given by

$$\Gamma = \frac{L}{r_{out} - r_{in}} \quad (2)$$

Various final modes of Taylor vortex flow are formed by changing these parameters.

3. PIV Analysis

PIV is a method used to quantify flows to enable their visualization. Figure 3 shows a schematic of the analytical method. A video of flows visualized using tracer particles is recorded using a high-speed video camera. The video sequences are segmented into frames of still images. The left and center images

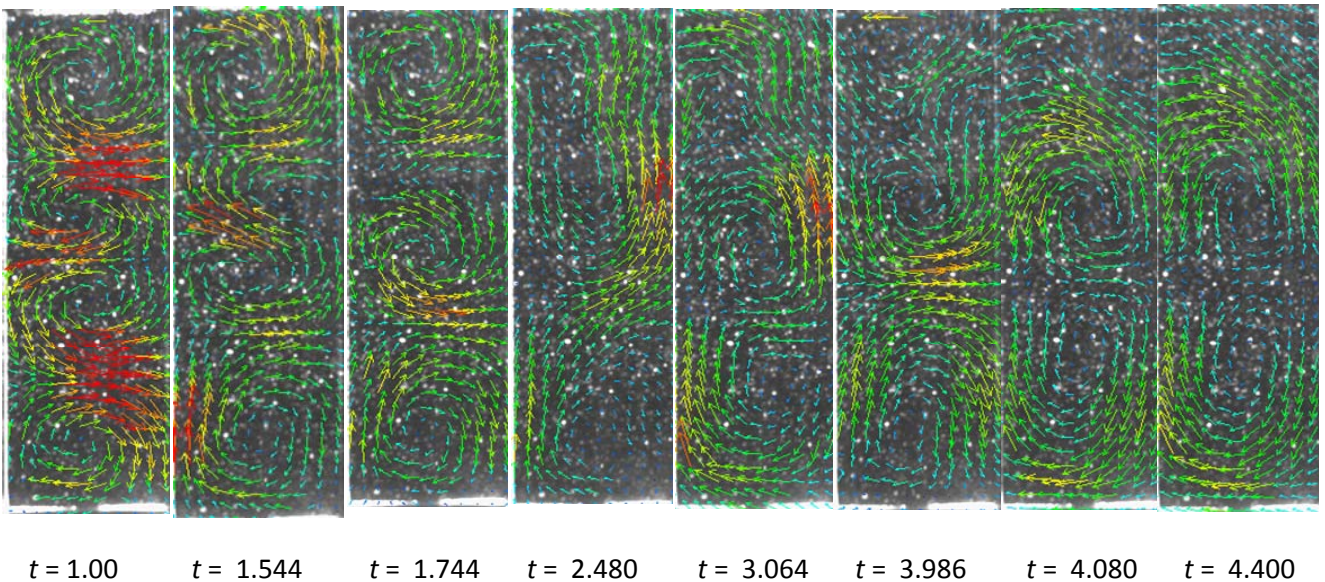


Fig. 5 PIV results ($Re = 1000 \rightarrow 300$, $\Gamma = 3.0$, 250 fps)



in Fig. 3 represent two successive extracted still images. Observing the movement of particles from time t_1 to t_2 reveals the velocity components in each still image, from which velocity vectors can be obtained.

4. Experimental Results

Transition from four-cell mode to two-cell mode In this study, using PIV we analyzed the transition from the normal four-cell (N4) mode to the normal two-cell (N2) mode when Γ was 3.0 as well as the transition from the normal six-cell (N6) mode to the N4 mode when Γ was 5.0. The results of PIV analysis for the former transition, obtained by recording at 250 fps, are described in this section. Figure 4 shows the change in Re with time during the transition. Re was decreased from 1,000 to 300 in 5 s. Figure 5 shows the results of PIV analysis for the flow during the transition. Recording was started 1 s after the rotation speed of the inner cylinder was changed ($t = 1$). In Fig. 5, warm-colored arrows represent high velocities, whereas cold-colored arrows represent low velocities. The images in Fig. 5 revealed that the transition of the vortices started at $t = 1.544$, and the three-cell mode was formed at $t = 1.744$. The flow underwent a transition to the two-cell mode at $t = 3.064$ and then to the N2 mode at $t = 4.4$. The transition of the vortices is explained as follows. First, the second vortex from the top disappeared to form the three-cell mode. Next, the central vortex absorbed the top vortex, which rotated in the same direction as the central vortex, to form the two-cell mode. Finally, the bottom vortex developed to form the N2 mode.

Measurement of size of extra vortex generated during transition The size of the extra vortex that appeared at the bottom-left corner of A1 when Re was 1,000 and Γ was 0.9 was measured. Compared with the conventional method, enlarged images can be obtained by combining a macro zoom lens and FLUOSTAR particles. The extra vortex was observed in $3 \times 3 \text{ mm}^2$ images, and the distances from the red dot to the red bars were measured, as shown in Fig. 6. Graphs of the radial and axial velocities of the extra vortex were not prepared. In 2011, Tanaka et al. estimated the size of the extra vortex to be approximately 2 mm from its images. Actual measurement in this study revealed that the axial and radial diameters were in the ranges of 0.7-1.02 and 1.09-1.89 mm, respectively. That is, the smallest extra vortex had an axial diameter of 0.7 mm and a radial diameter of 1.09 mm, whereas the largest extra vortex had an axial diameter of 1.02 mm and a radial diameter of 1.89 mm. It was confirmed that the extra vortex that was generated had a height of approximately 10% of the cylinder length (9 mm) and a width of approximately 11-19% of the gap width (10 mm). Therefore, the diameter of the extra vortex was not considered to exceed 2 mm.

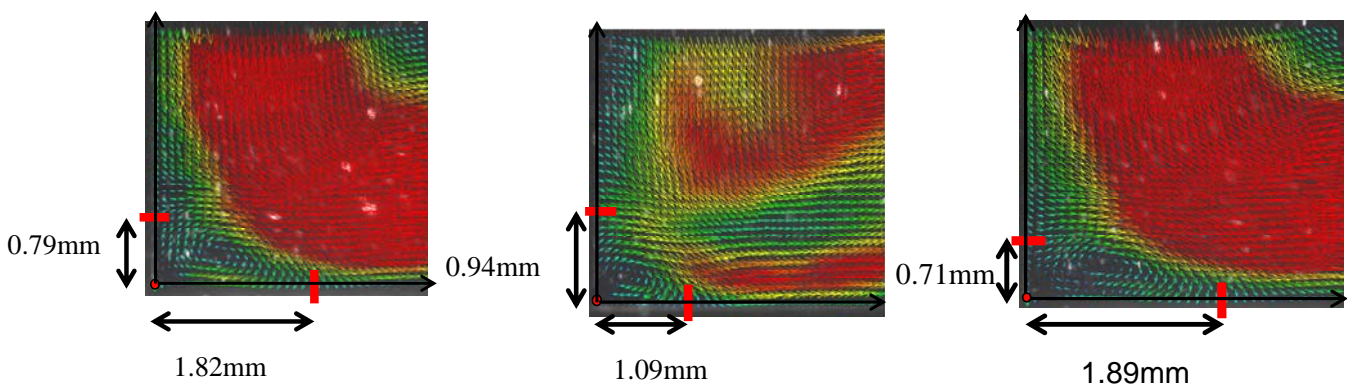
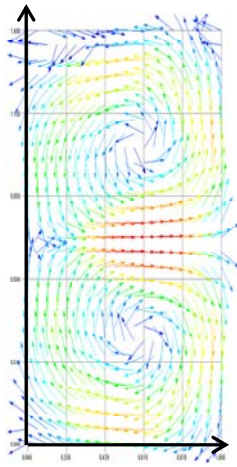
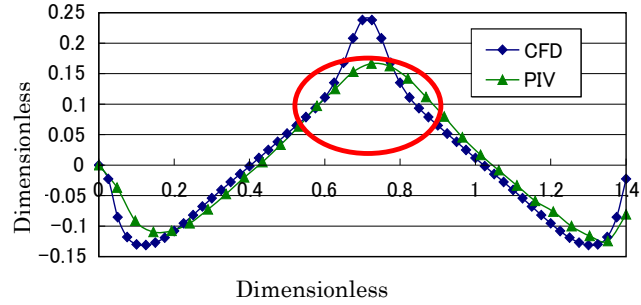


Fig. 6 PIV results for extra vortex ($Re = 1000$, $\Gamma = 0.9$, 250 fps)

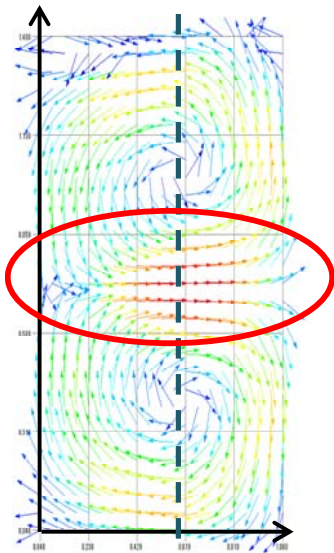


(1) Normalized PIV result

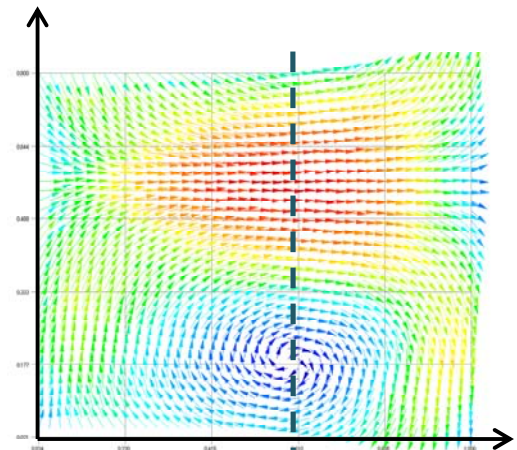


(2) Dimensionless velocity

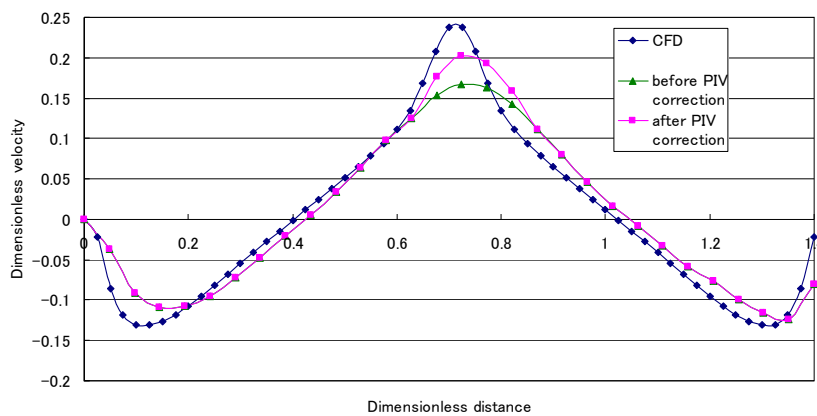
Fig. 7 PIV results before improvement ($Re = 1400, \Gamma = 1.4, 250\text{fps}$)



(1) Normalized PIV result



(2) Normalized PIV result for red circle



(3) Velocity distribution after correction



The variation in the size of the extra vortex, as observed in this study, may be due to the effect of the neighboring large vortex that exists above the extra vortex. The radial and axial velocities at the center of the extra vortex will be obtained by furthering this study in the future.

5.Improvement of accuracy: N2 mode

Figure 7 shows the results reported by Tanaka et al. in 2011. The values in the area enclosed by the red circle had large errors and were corrected as shown in Fig. 8. The area enclosed by the red circle, i.e., the area with high velocities, was enlarged to obtain the right-hand image in Fig. 8. The maximum dimensionless velocity was 0.238 at a dimensionless distance of approximately 0.7 according to the results of a computational fluid dynamics (CFD) simulation, whereas it was 0.1645 at approximately 0.8 according to the results of PIV analysis before correction. The difference between them was 0.0735, giving an error of 30.9%. When the result of PIV analysis was corrected, the maximum dimensionless velocity became 0.1978 at a dimensionless distance 1.0. The error was 16.9%, which was 14% smaller than the error before correction. Therefore, enlarging the area with high velocities in the analysis can reduce the error and increase the accuracy of analysis.

6.Improvement of accuracy: N6 mode

The accuracy of analysis for the N6 mode was improved by enlarging two areas as shown in Fig. 9. The maximum dimensionless velocity in red circle 1 obtained by the CFD simulation was 0.281, whereas it was 0.111 at a dimensionless distance of approximately 1.0 according to the results of PIV analysis before correction. The difference between these values was 0.17, giving a large error of 60.5%. After the correction of the PIV analytical result, the maximum dimensionless velocity became 0.219 at the same dimensionless distance of approximately 1.0, a difference of 0.062 from the value obtained by the CFD simulation. The error was 22.1%, which was over 35% smaller than the error before correction. The minimum dimensionless velocity in red circle 2 obtained by the CFD simulation was -0.177, whereas it was -0.12 according to the results of PIV analysis before correction. The difference between these values was 0.057, giving an error of 32.2%. After the correction of the PIV analytical result, the minimum dimensionless velocity became -0.17, a difference of 0.007 from the result of the CFD simulation. The error was 4%, indicating that the PIV result after correction was in good agreement with that obtained by the CFD simulation. From above, the accuracy for targets observed with a large aspect ratio can be markedly improved by first analyzing the flow throughout the target then analyzing enlarged images of the area between vortices.

7.Conclusions

Transition from four-cell mode to two-cell mode We analyzed the transition from the N4 mode to the N2 mode and that from the N6 mode to the N4 mode and successfully analyzed the unsteady flows in detail. In the transition from the N6 mode to the N4 mode, the second vortex from the top disappeared and one of the vortices was absorbed by another vortex with the same rotation direction. The process of disappearance of the vortex in the transition from the N4 mode to the N2 mode was considered to be similar to that in the transition from the N6 mode to the N4 mode.

In the experiment, only the above-mentioned transitions were observed. However, different transition processes were also observed in the numerical simulation, which should have also been observed in the experiments. Although an abrupt change in the rotation speed of the inner cylinder was required to

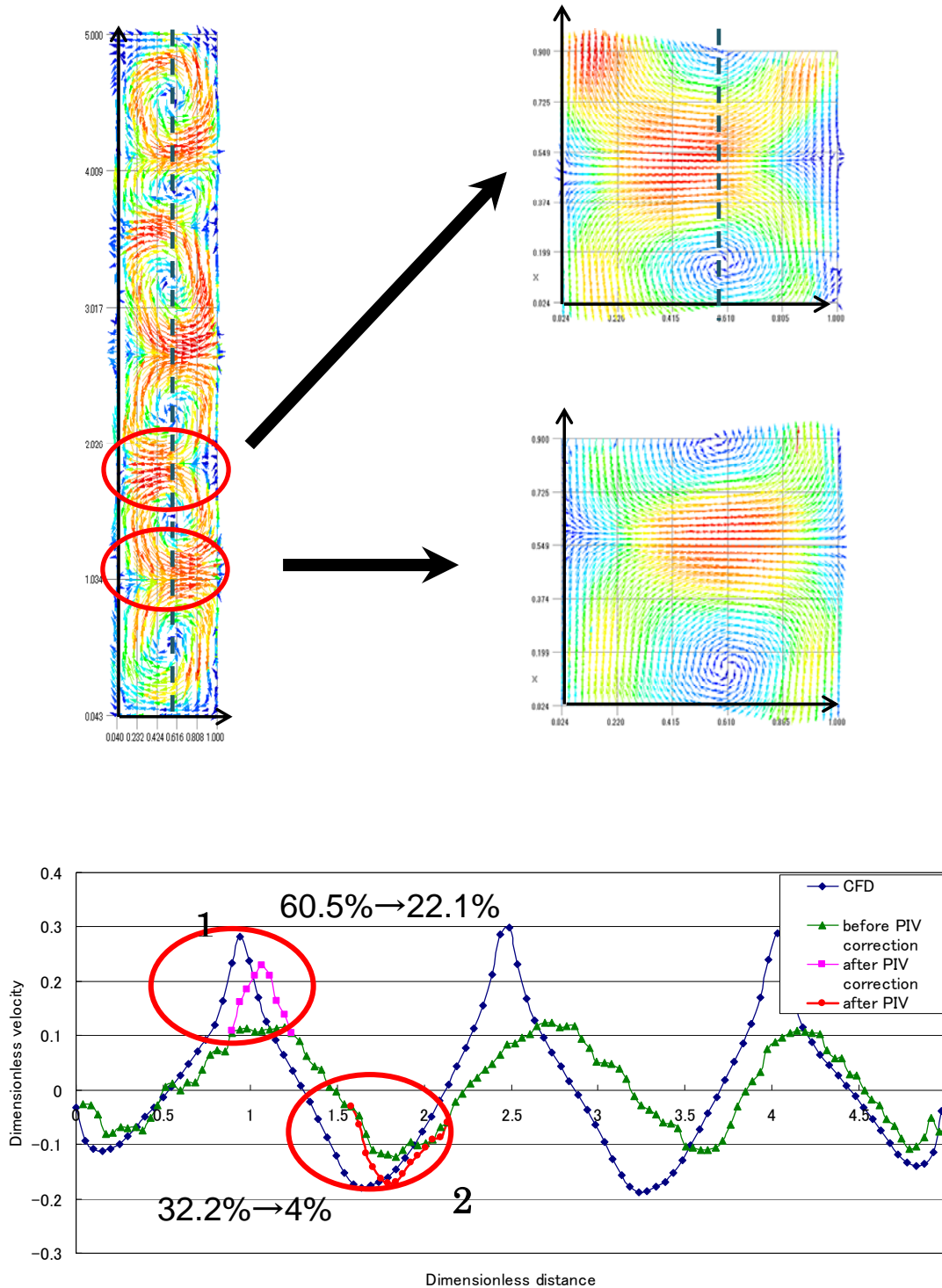


Fig. 9 Improvement of accuracy (N6, $Re = 1000$, $\Gamma = 5.0$, 250fps)

induce the transition of flows in this study, it was considered that transitions other than those mentioned above can also be experimentally observed by gradually changing the rotation speed of the inner cylinder.

References

- (1) Taylor G. I., Stability of a Viscous Liquid Contained between Two Rotating Cylinders, Phil. Trans. Roy. Soc. Lond, A233, 1923, pp.289-343.
- (2) Tagg, R., The Couette-Taylor problem, Nonlinear Science Today, 4-3, 1994, pp.1-25.
- (3) Special issue, Taylor-Couette flows, Theoretical and Computational Fluid Dynamics 16-1, 2002.



- (4) Cliffe, K.A., Numerical calculation of two-cell and single cell Taylor flow, *J. Fluid Mech.*, 135, 1983, pp.219-233.
- (5) Cliffe, K.A., Numerical calculation of the primary flow exchange process in the Taylor problem, *J. Fluid Mech.*, 197, 1988, pp.57-79.
- (6) Bolstad, J. H. and Keller, H. B., Computation of anomalous modes in the Taylor experiment, *J. Comput. Phys.*, 69, 1987, pp.230-251.
- (7) Benjamin, T. B. and Mullin, T., Anomalous mode in the Taylor experiment, *Proc. R. Soc. Lnd. Ser. A*, 377, 1981, pp.221-249.
- (8) Cliffe, K. A and Mullin, T. "A numerical and experimental study of anomalous modes in the Taylor experiment" *J. Fluid Mech.*, 153, pp. 243-258, 1985.
- (9) Benjamin, T. B., Bifurcation phenomena in steady flows in a viscous flow - II . Experiment-, *Proc. R. Soc. Lnd. Ser. A*, 359, 1979, pp.27-43.
- (10)Lücke, M., Mihelcic, M., and Wingerath, K., and Pfister, G., Flow in a Small Annulus between Concentric Cylinders, *J. Fluid Mech.*, 140 1984, pp. 343-353.
- (11)Lücke, M., Mihelcic, M., and Wingerath, K., Front propagation and pattern formation of Taylor vortices growing into unstable circular coquette flow, *Phy. Rev A*, 31-1, 1985, pp.396-409
- (12)Kuo, D. C. and Ball, K. S., Taylor-Couette flow with buoyancy: onset of spiral flow, *Phys. Fluids*, 9-10, 1997, pp.2872-2884.
- (13)Bielek, C. A. and Koschmieder, E. L., Taylor vortices in short fluid columns with large radius ratio, *Phys. Fluids A*, 2-9, 1990, pp.1557-1563.
- (14)Benjamin, T.B. and Mullin, T., Notes on the multiplicity of flows in the Taylor experiment, *J. Fluid Mech.*, 121, 1982, pp.219-230
- (15)Alziary de Roquefort, T. and Grillaud, G., Computation of Taylor vortex flow by a transient implicit method, *Comput. Fluids*, 6, 1978, pp.259-269.
- (16)Cliffe, K. A. and Mullin, T., A numerical and experimental study of anomalous modes in the Taylor experiment, *J. Fluid Mech.*, 153, 1985, pp.243-258.
- (17)Furukawa, H., Watanabe, T., Nakamura, I., Visual information of the mode formation in accelerating Taylor vortex flow with finite length, *Proc. 9th Int. Symp. Flow Visual.*, 2000.
- (18)Neizal, G. P., Numerical computation of time dependent Taylor-vortex flows in finite-length geometries, *J. Fluid Mech.*, 141, 1984, pp.51-66.
- (19)Liao, C. B., Jane, S.J., and Young, D. L., Numerical simulation of three-dimensional Couette-Taylor flows, *Int. J. Numer. Meths. Fluids*, 29, 1999, pp.827-847.



(20) Fasel, H. and Booz, O., Numerical investigation of supercritical Taylor-vortex flow for a wide gap, J. Fluid Mech., 138, 1984, pp.21-52.